主办 中国科学院遥感与数字地球研究所
中国地理学会环境遥感分会
出版 科学出版社

JOURNAL OF REMOTE SENSING

遥感学报

2013年 Vol.17 第17卷 No.4 第4期 ISSN 1007-4619 CN11-3841 / TP CODEN YXAUAB

2010年中国土地覆被遥感监测数据集（ChinaCover2010）

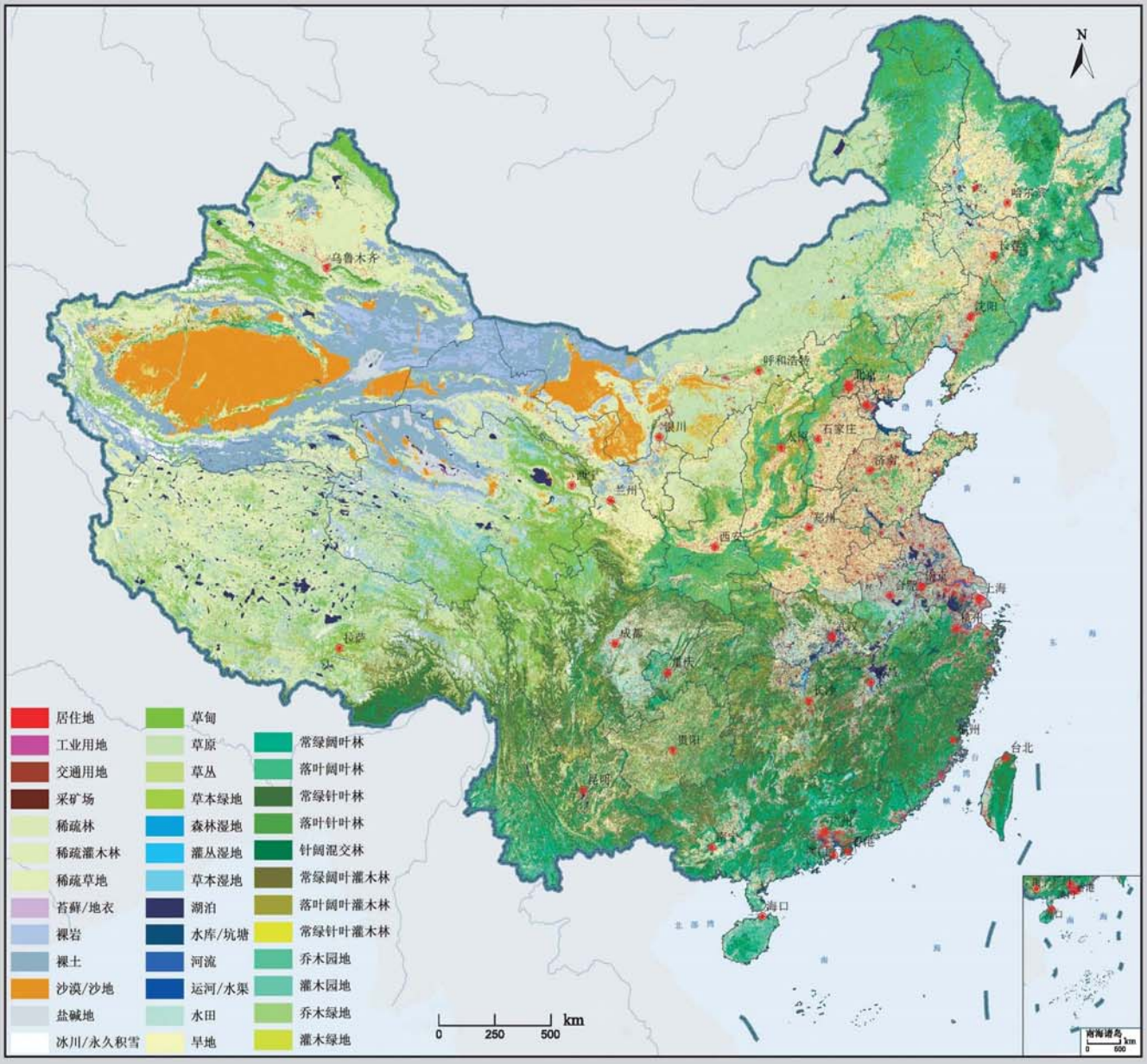

百种中国杰出学术期刊

遥感学报

Yaogan Xuebao

第 17 卷　　第 4 期　　2013 年 7 月

目　　次

JOURNAL OF REMOTE SENSING

(Vol. 17 No. 4 July, 2013)

CONTENTS

(to be continued to Inside Back Cover)

(continued from Contents page)

Haze: Remote Sensing

Retrieval of haze aerosol optical depth based on high spatial resolution CCD of HJ-1

ZHANG Yuhuan[1,2], LI Zhengqiang[1], HOU Weizhen[1], XU hua[1]

1. *State Environmental Protection Key Laboratory of Satellites Remote Sensing, Institute of Remote Sensing and Digital Earth of Chinese Academy of Sciences, Beijing* 100101, *China*;
2. *University of Chinese Academy of Sciences, Beijing* 100049, *China*

Abstract: Haze pollution becomes more and more frequent in urban regions of China. Compared to ground based measurement approaches, satellite remote sensing can obtain observation of haze in wide areas and monitor their distribution and intensity. The Chinese environmental satellites of HJ-1A and HJ-1B play important roles in atmosphere monitoring due to their high spatial resolution, high temporal resolution and wide swath. In this paper, aerosol optical depth during haze in January 2013 is retrieved using HJ-1 CCD blue and green bands based on the assumption of stable surface reflectance in a short period. Applications of HJ-1 CCD haze monitoring are also evaluated and feasibility and advantages of the high-resolution satellite are analyzed.

Key words: high spatial resolution, aerosol optical depth, Beijing, haze, HJ-1 CCD

CLC number: TP751 **Document code**: A

Citation format: **Zhang Y H, Li Z Q, Hou W Z and Xu H. 2013. Retrieval of haze aerosol optical depth based on high spatial resolution CCD of HJ-1. Journal of Remote Sensing, 17(4): 959-969 [DOI: 10.11834/jrs.20133062]**

1 INTRODUCTION

Haze is an aerosol system which consists of atmospheric particles such as soot and dust in specific humidity and temperature. The sizes of the aerosol particles distribute mainly between 0.1 μm and 10 μm which can come from human sources such as industrial emissions, construction, waste incineration, waste gas, vehicle exhaust and natural source, such as sand dust, volcanic eruptions, and forest fires (Ma,et al., 2008). Haze is identified, by the International Meteorological Organization (WMO), as the weather when air relative humidity is less than 80% and the level of visibility is less than 10 km. According to the visibility, haze can be divided into three levels: heavy haze (visibility ≤ 2 km), moderate haze (2 km < visibility ≤ 5 km) and light haze (5 km < visibility ≤ 10 km).

At present, the haze in China is very serious and prevails in many cities and towns. There are four typcial hazy areas in China: the Pearl River Delta, the Yangtze River Delta, the Huang-Huai-Hai region and the Sichuan Basin. Haze is a severe disastrous weather phenomenon which increasingly impacts on environment and human health. It can cause human respiratory and lung diseases. It can also reduce atmospheric visibility and affect air quality in urban, hence resulting in the reduction of solar radiation intensity and sunshine hours, and even agricultural production (Li & Yu, 2011).

Environmental protection departments concern mainly about the concentration of respirable particulate matters and polluting gases such as NO_2 and SO_2, which affect the air quality near ground surface in haze days. The monitoring near ground in a point scale can indicate the status of haze pollution nearby. However, the large-scale monitoring is absent (Li, 2010). It is difficult to obtain the trend of haze distribution and intensity in a large area at present. Due to wide coverage and efficiency of data, satellite remote sensing is a fast approach to obtain regional haze aerosol optical depth for atmospheric environment monitoring.

The approaches for aerosol remote sensing over land can be divided into four main categories: (1)Dark target method which has been successfully applied to the Moderate-Resolution Imaging Spectroradiometer (MODIS) aerosol retrieval (Levy, et al., 2007) based on the relationship of shortwave infrared channel (2.12 μm), red channel (0.66 μm) and blue channel (0.47 μm); (2) Multi-angle method which is adopted by the Multi-angle Imaging Spectroradiometer (MISR) (Martonchik, et al., 1992) based on observation of the multi-angle; (3) Contrast reduction method based on the surface reflectance (Tanre, et al., 1998); (4) The Polarized aerosol retrieval method based on the polarization information (Polarization and Directionality of the Earth's Reflectances: POLDER) (Deuzé, et al., 2001).

Received: 2013-03-21; **Accepted**: 2013-05-10; **Version of record first published**: 2013-05-17

Foundation: Key Project of Scientific and Technological Innovation of the Chinese Academy of Sciences (No.KGFZD-125-13-006); National Major Scientific Research Program (No.2010CB950800, 2010CB950801)

First author biography: ZHANG Yuhuan (1984—), female, Ph.D. candidate, she majors in remote sensing of atmosphere. E-mail: zhangyh@irsa.ac.cn

Corresponding author biography: LI Zhengqiang (1977—), male, professor, his research interest is environment remote sensing research. E-mail: lizq@irsa.ac.cn

HJ-1A/1B satellites (The China Environment and Disasters Monitoring Microsatellite Constellation) launched in 2008 are dedicated to the environment and disaster monitoring and forecasting. The CCD sensors have three visible bands (430—520 nm, 520—600 nm, 630—690 nm) and a near-infrared band (760—900 nm) with 30 m spatial resolution, 360 km swath for each (700 km when jointly used) and 4 days revisit period for each (2 days when jointly used). The high temporal resolution, spatial resolution and wide coverage characteristics enable HJ-1 satellites to be suitable for atmospheric monitoring. Therefore, the atmosphere environmental monitoring and remote sensing studies based on HJ-1 are in great interests (Wang,et al., 2010). Li (2010) discussed the cloud recognition and Aerosol Optical Depth (AOD) retrieval method of haze using MODIS and HJ-1 CCD data respectively. Wang,et al. (2012) also used HJ-1 CCD data of environment satellites to study the haze phenomenon in Beijing during 2009. Xu, et al. (2013) gave a brief presentation of AOD on both haze (January 14) and clear (January 17) days in 2013. This paper focuses on the aerosol retrieval method and the multi-temporal AOD results using CCD images of HJ-1 satellites during Beijing 2013 haze process, and compares the retrieval results with the low resolution MODIS aerosol products.

2 METHOD AND ALGORITHM

2.1 Method basis

Satellite remote sensing of AOD relies on the reflectance at the top of atmoshpere (TOA). Assuming a Lambertian surface and no gas absorption, the apparent reflectance of satellite observation can be written as

$$\rho_{\mathrm{TOA}}(\mu_s,\mu_v,\varphi) = \rho_o(\mu_s,\mu_v,\varphi) + \frac{T(\mu_s)T(\mu_v)\rho_s(\mu_s,\mu_v,\varphi)}{1-\rho_s(\mu_s,\mu_v,\varphi)S} \tag{1}$$

where ρ_{TOA} is reflectance at TOA, θ_v and θ_s are solar zenith angle and viewing zenith angle respectively, $u_v=\cos\theta_v$, $u_s=\cos\theta_s$, ρ_0 is the normalized atmospheric path reflectance, T is atmospheric transmission, S is the atmospheric albedo, and ρ is the Lambertian reflectance.

Atmospheric transmittance can be divided into transmitted part and scattering parts:
$T(\mu)=\mathrm{e}^{-\tau/\mu}+t_d(\mu)$, where τ is total aerosol optical depth, and t_d is scattering transmittance.

The total radiance which is received by satellite sensor contains both surface and atmosphere information, and the path radiance mainly from the atmospheric contribution.

Removal of underlying surface reflectance from total reflectance is the key technique of AOD retrieval. In this paper, we use 6S (Second Simulation of Satellite Signal in the Solar Spectrum) Radiance Transfer (RT) model to simulate the reflectcance that received by satellite, and separate it into surface and atmoshpere reflectances based on some assumed of surface reflectance to acquire AOD from satellite observation.

2.2 HJ-1 AOD retrieval method

The retrieval algorithm of AOD is based on two assumptions (Hagolle, et al., 2008): (1) Aerosol optical properties vary quickly with time but slowly with location, and thus AOD in our research is assumed to be invariable within a small study area. (2) Surface reflectance varies quickly with location but slowly with time, and thus we can consider a stable surface reflectance in a short time. Based on the two assumptions, the differences of apparent radiance between two images (in a short time: e.g., 2 days) are mostly considered to be the contribution of aerosols. Therefore, we can get the surface reflectance and correspondingly AOD from the variation of TOA reflectance based on the stablity of surface reflectance.

The processing of AOD retrieval is as follows.

(1) The Look-up Table (LUT) is precalculated for a given location, sensor and time. In this paper, the LUT is bulit using 6S radiative transfer model. Parameters (e.g. solar zenith angle, viewing zenith angle, relative azimuth angle, aerosol optical depth, surface reflectance) are considered in the LUT. Meanwhile, the atmospheric models (Midlatitude Summer, Midlatitude Winter, etc) and aerosol models (Continental, Urban, etc) in 6S are used.

The difference in AOD retrievals' for weak and haze aerosol mainly lies on the selection of parameters of aerosol models. Previous studies show that (Li, et al., 2013) the parameters of aerosol model in haze days are similar with those of continental aerosol model and with higher aerosol concertration. Therefore, continental aerosol model is selected in this paper.

(2) Using a constant aerosol model with different aerosol optical depth, we can get the surface reflectance related to the AOD by the LUT.

(3) The surface reflectance and corresponding AOD approach to the real values when the surface reflectance differences between two adjacent images are minimized.

The following cost function (Hagolle, et al., 2008) is used to calculate the difference of surface reflectance.

$$\begin{aligned} Cost = {} & K\sum_{i,j,\lambda}\left(atm_{\mathrm{cor}}(L_{\mathrm{TOA}}(i,j,\lambda,D1),\mathrm{AOD}(D1)) - atm_{\mathrm{cor}}(L_{\mathrm{TOA}}(i,j,\lambda,D2),\mathrm{AOD}(D2))\right)^2 + \\ & \sum_{i,j,\lambda}\left(atm_{\mathrm{cor}}(L_{\mathrm{TOA}}(i,j,\lambda,D1),\mathrm{AOD}(D1)) - \rho_{\mathrm{surf}}(i,j,\lambda,D1)\right)^2 + \\ & \sum_{i,j,\lambda}\left(atm_{\mathrm{cor}}(L_{\mathrm{TOA}}(i,j,\lambda,D2),\mathrm{AOD}(D2)) - \rho_{\mathrm{surf}}(i,j,\lambda,D1)\right)^2 \end{aligned} \tag{2}$$

where λ is the wavelength, (i,j) are the coordinates of neighborhood pixels, and we assume the aerosol is constant in this neighborhood. ρ_{surf} is the initial surface reflectance, L_{TOA} is TOA radiance, atm_{cor} is the atmospheric model that enables estimate the surface reflectance from TOA reflectance. $D1$ and $D2$ represent imaging date. K is a weighting coefficient which is proportional to the average variation of L_{TOA} between $D1$ and $D2$. Assuming that the selected images of $D1$ and $D2$ in the selected area are cloudless, and surface reflectances are stable in a short period, we can obtain the AOD in $D1$ and $D2$ and the corresponding surface reflectance by minimizing the cost funtion in Eq.(2).

The CCD sensors of HJ-1 have three visible bands and one near-infrard band. The blue and green bands, centered at 483 nm and 568 nm, are employed for the inversion since they are sensitive to aerosols. In most of cases, the surface reflectance of these bands varies slowly (Hagolle & King, 2008). In this paper, we use these two bands to derive AOD. The spectral response functions of four bands are shown in Fig.1.

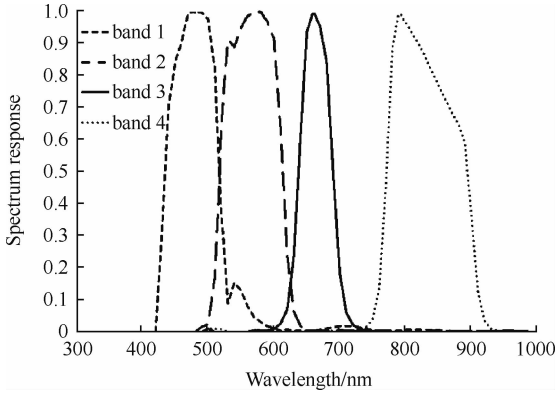

Fig.1 Spectral response functions of HJ-1 (adopted from HJ-1 A CCD1)

2.3 Cloud identification

Haze pixel must be recognized before AOD retrieval. Meanwhile, the accuracy is directly affected by the identification of haze, cloud, and surface pixels. Many satellite sensors have mature algorithms for cloud identification which in not the case of HJ-1 CCD. Considering that CCD sensors of HJ-1 only have three visible bands and one near infrared band, we use threshold values [0.07, 0.25] in blue band and [0.1, 0.28] in green band to identify clouds. These threshold ranges can exclude most of thick clouds and prevent misjudgment of the heavy haze or bright surface into clouds (Ackerman, et al., 2010; Li, 2010). The cloud data is identified and removed by using this sample threshold method, and then AOD will be not retrieved in the case of cloud.

3 RESULTS AND DISCUSSION

3.1 Data selection and processing

Six images of HJ-1 CCD in haze days from January 8 to 17, 2013 (Table 1) are selected. The image on January 8 shows the beginning of haze. The Air Quality Index (AQI) is 158 on Agricultural Exhibition Hall site in Beijing during this day. The images on January 12 and 14 show the heavy haze polution of the process. In those days, the AQI are 500 and 293, respectively. The image on January 17 is obtained after haze dispersing with the AQI of about 106. Series images shows the whole haze process of generation, development, accumulation and dispersion in Beijing.

Table 1 Selection of data in 2013 at Beijing

Date	Sensor	Transit time
2013-01-08	HJ-1A CCD1	02:37
2013-01-10	HJ-1B CCD1	02:36
2013-01-12	HJ-1A CCD1	02:42
2013-01-14	HJ-1B CCD1	02:41
2013-01-16	HJ-1A CCD1	02:46
2013-01-17	HJ-1B CCD2	02:20

After geocorrection and resizing of images, we select the 20 × 20 km^2 study area in Beijing, which contains about 666 × 666 pixels in HJ CCD images (with 30 m spatial resolution). Fig.2 shows the false color image of the study area. In this figure, the red box represents location of ground-based CE318 sun photometer at the Institute of Remote Sensing and Digital Earth(RADI).

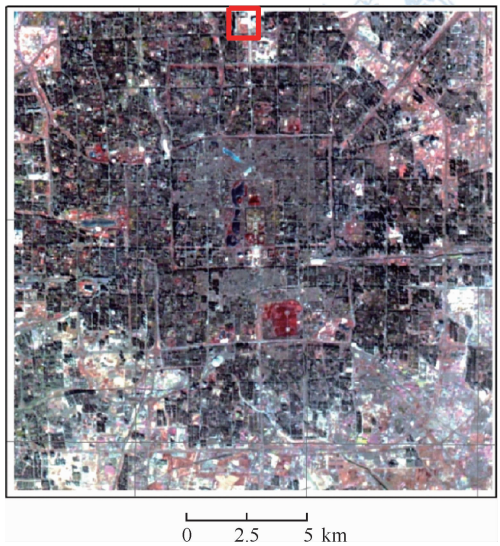

Fig.2 Study area of HJ-1 CCD (area: 20×20 km^2)

HJ-1 CCD images are then resampled into 100 m resolution (200 × 200 pixels) in order to reduce the noise, geometric registration errors, as well as local variation of surface reflectance. Then, we can acquire images of TOA (Top of Atmosphere) signal after radiance calibration. AOD is considered to be constant in the 5 × 5 pixels area (0.5 × 0.5 km^2), so the maximum i and j are both 5 in Eq.(2), i.e., the spatial resolution of AOD result is 500 m.

3.2 HJ-1 AOD retrieval results

Fig.3 shows AOD results in haze days from January 8 to 17 in Beijing. The initial surface reflectance in this method is obtained from the atmospheric correction data of the first day in the time series (January 8, 2013). The values of zero in AOD results on January 10 and 12, 2013 are invalid, which is attributed to residuals cloud contamination.

Combining HJ-1A and HJ-1B, we can get AOD data in every two days. Therefore, we can investigate haze process, including generation, development, accumulation and dispersion.

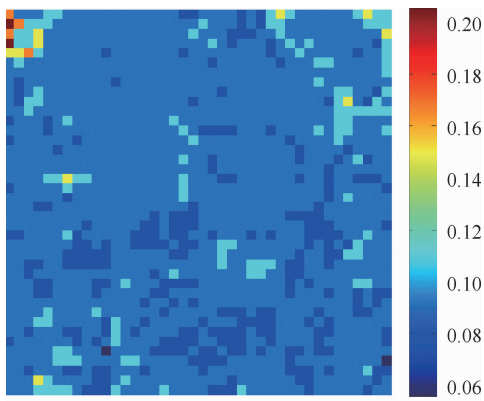

(a) 2013-01-08

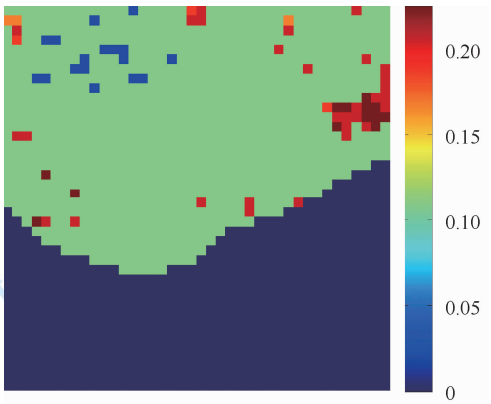

(b) 2013-01-10

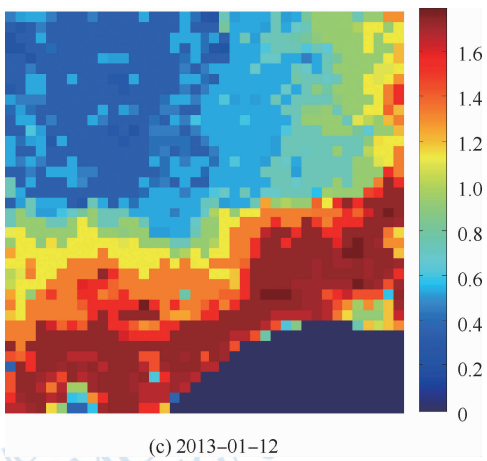

(c) 2013-01-12

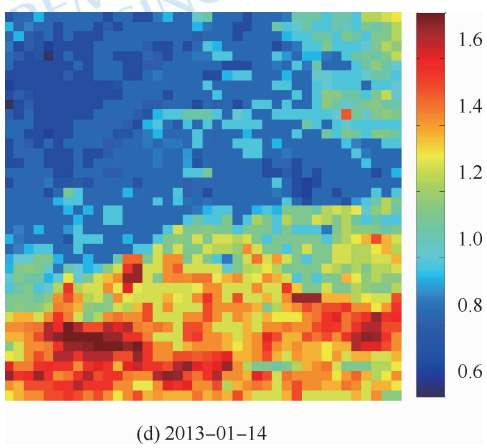

(d) 2013-01-14

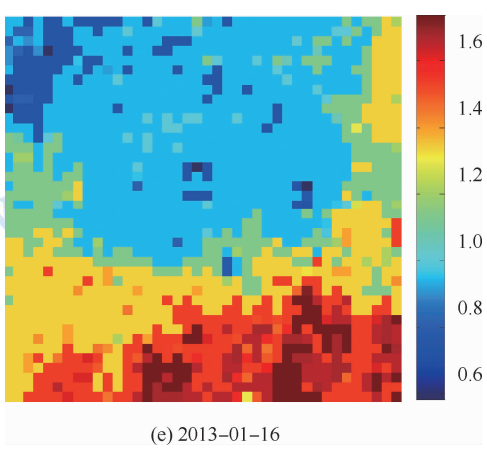

(e) 2013-01-16

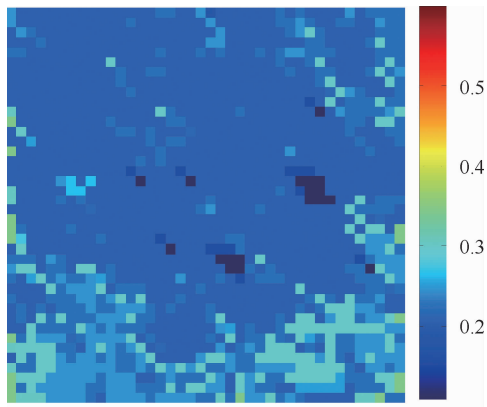

(f) 2013-01-17

Fig.3 AOD series from January 8 to 17, 2013

We draw conclusions from the above results: The image on January 8 is the beginning of the haze with the mean AOD of about 0.1, and the differences of AOD among pixels in the whole study area are small (less than 0.15). January 10 is the developing period of the haze. Although the south area is cloudy, AOD in north area is higher than that on January 8 obviously, which illustrates the accumulation of the haze. The AOD continues to increase on Januray 12, which is higher than that on January 10 totally. AOD in the south city is higher than that in the north and the biggest difference between south and north reach to 1.4, which represents the most serious haze pollution day. January 14 is another serious haze day. Due to spreading of haze to the north, the AOD results in north city becomes higher than the results on January 12 obviously, and the biggest difference between south and north reaches to 1.6. That is similar with the result of January 12. The haze begins to disappear during January 16, and AOD has a significant decline compared with the result of January 14. The value of AOD decreases from 1.7 (January 14) to 1.4 (January 16) in north area, and from 0.9 (January 14) to 0.6 (January 16) in south area. The haze disappears on January 17 and AOD is less than 0.35 in the whole area.

3.3 Validation

(1) Validation of the retrieved AOD.

AOD at 550 nm is calculated by Angstrom exponent (Dubovik, et al, 2000; Ångström, 1929) which is acquired from CE318 observation (the site of Institute of Remote Sensing and Digital Earth Institute) at 440 and 870 nm. Ångström equation used in this work is shown blow (Eq.(3)).

$$\tau_\alpha(\lambda) = \beta\lambda^{-\alpha} \tag{3}$$

where, $\tau_\alpha(\lambda)$ is aerosol optical depth at wavelength λ, β is turbidity factor, and α is band index, which indicates the particle size. The smaller α means the larger aerosol particles.

The observed AOD at 550 nm is then compared with the retrieved AOD from HJ-1 CCD data. Here, Level 2.0 AErosol RObotic NETwork (AERONET) AOD is used as validation data, which is acquired at the HJ-1 transit time, i.e. averaged for the period before and after half an hour of satellite transit time.

Table 2 shows the verification results. The mean difference between the retrieved AOD and CE318 observed AOD during 6 days is about 0.002. The maximum error is 0.252 which occurs

on January 10, and the minimum error is 0.007 which occurs on January 14. The correlation equation between CE318 and HJ-1 CCD AOD is: $\tau_{HJ}=1.083\times\tau_{CE318}-0.030$, $R^2=0.84$.

Table 2 Verification of HJ-1 CCD AOD retrieval results

Date	CE318-AOD	HJ-1 AOD	Error
2013-01-08	0.102	0.074	0.026
2013-01-10	0.412	0.160	0.252
2013-01-12	0.365	0.420	0.055
2013-01-14	0.858	0.940	0.082
2013-01-16	0.467	0.560	0.093
2013-01-17	0.138	0.200	0.062
Mean	0.390	0.392	0.095

(2) Comparison between retrieved AOD and MODIS AOD production

Haze is often misjudged as light cloud, fog or bright surface in MODIS cloud masking and aerosol products (King, et al., 2003; Liang, et al., 2006), so that there are many inaccurate or missing values in MODIS aerosol products. MOD08 (the MODIS Level 3 daily, 8-day and monthly atmospheric product in a spatial resolution of 1km) products during January, 2013 have rare valid values compared with our results, which limits significantly the application of MODIS data in the haze monitoring.

4 CONCLUSION

AOD retrieval from HJ-1 satellites shows the process of haze generation, development, accumulation and dispersion in January in Beijing. The advantages of HJ-1 CCD observation such as high spaital and time resolution make it suitable for haze monitoring . From above analysis our conclusions are as follows.

(1) In the haze days from January 8 to 17, 2013 in Beijing, the haze spreads from north to south area. January 8 and 10 are the process of haze development, and January 12 and 14 are serious pollution days. Haze begins to disperse on January 16, and January 17 it becomes a clear day.

(2) From the AOD results of January 12 and 14, 2013, it is found that haze spreads from south to north area in Beijing, while the south area is more polluted than north area. The haze expands from the south, and gradually surrounds the northern area. The AOD in south area is higher than that in north significantly.

Satellite remote sensing can be an effective complement to the ground observation. It can provide real-time and fast monitoring of haze, and provide the influence, severity and distribution of haze.

Acknowledgements: The authors gratefully thank Beijing Municipal Environmental Protection Bureau for providing the AQI data.

REFERENCES

A Ackerman S, Frey R, Strabala K, Liu Y, Gumley L, and Baum B. 1998. Discriminating clear sky from clouds with MODIS. Journal of Geophysical Research: Atmospheres (1984 – 2012), 103(D24): 32141-32157

Ångström A. 1929. On the atmospheric transmission of sun radiation and on dust in the air. Geografiska Annaler, 11: 156-165

Deuzé J L, Bréon F M, Devaux C, Goloub P, Herman M, Lafrance B, Maignan F, Marchand A, Nadal F, Perry G and Tanré D. 2001. Remote sensing of aerosols over land surfaces from POLDER-ADEOS-1 polarized measurements. Journal of Geophysical Research, 106(1996): 4913-4926 [DOI: 10.1029/2000JD900364]

Dubovik O and King M D. 2000. A flexible inversion algorithm for retrieval of aerosol optical properties from sun and sky radiance measurements. Journal of Geophysical Research, 105(D16): 20673-20696 [DOI: 10.1029/2000JD900282]

Hagolle O, Dedieu G, Mougenot B Debaecker V, Duchemin B and Meygret A. 2008. Correction of aerosol effects on multi-temporal images acquired with constant viewing angles: Application to Formosat-2 images. Remote Sensing of Environment, 112(4): 1689 – 1071 [DOI: 10.1016%2fj.rse.2007.08.016]

King M D, Menzel W P, Kaufman Y J, Tanre D, Platnick S, Ackerman S A, Remer L A, Pincus R and Hubanks P. 2003. Cloud and aerosol properties, precipitable water, and profiles of temperature and water vapor from MODIS. IEEE Transactions on Geoscience and Remote Sensing, 41(2): 442-458 [DOI: 10.1109/TGRS.2002.808226]

Levy R C, Remer L A, Mattoo S, Vermote E F and Kaufman Y J. 2007. Second-generation operational algorithm: retrieval of aerosol properties over land from inversion of Moderate Resolution Imaging Spectroradiometer spectral reflectance. Journal of Geophysical Research, 112(D13): 1-21 [DOI: 10.1029/2006JD007811]

Liang S L, Zhong B and Fang H L. 2006. Improved estimation of aerosol optical depth from MODIS imagery over land surfaces. Remote Sensing of Environment, 104(4): 416-425

Li S S. 2010. Study on the Retrieval of Haze Aerosol Optical Thickness using Satellite Data. Graduate School of Chinese Academy of Sciences

Li X M and Yu X N. 2011. Research progresses on aerosol chemical properties during haze episodes. Sciencepaper Online, 6(9): 661-664

Li Z Q, Gu X, Wang L, Li D, Li K, Dubovik O, Schuster G, Goloub P, Zhang Y, Li L, Xie Y, Ma Y and Xu H. 2013. Aerosol physical and chemical properties retrieved from ground-based remote sensing measurements during heavy haze days in Beijing winter. Atmospheric Chemistry and Physics Discussions, 13(2): 5091-5122 [DOI: 10.5194/acpd-13-5091-2013]

Ma G X, Xue Y Q and Li G F. 2008. Satellite remote sensing for haze monitoring in pear l river delta region. Science and Technology Review, 26(16): 72-76

Martonchik J V and Dine D J. 1992. Retrieval of aerosol optical properties from multi-angle satellite imagery. IEEE Transactions on Geoscience and Remote Sensing, 30(2): 223-230 [DOI:10.1109/36.134073]

Tanre D, Deschamps P Y, Devaux C and Herman M. 1988. Estimation of Saharan aerosol optical thickness from blurring effects in Thematic Mapper data. Journal of Geophysical Research, 93(D12): 15955-15964 [DOI: 10.1029/JD093iD12p15955]

Vermote E F, Tanre D, Deuze J L, Herman M and Morcette J J. 1997. Second simulation of the satellite signal in the solar spectrum, 6S: an overview. IEEE Transactions on Geoscience and Remote Sensing, 35(3): 675-686 [DOI: 10.1109/36.581987]

Wang Q, Wu C Q and Li Q. 2010. Environment Satellite 1 and its application in environmental monitoring. Journal of Remote Sensing, 14(1): 104-121

Wang Z T, Li Q, Li S S, Chen L F, Zhou C Y, Wang Z F and Zhang L J. 2012. The monitoring of haze from HJ-1. Spectroscopy and Spectral Analysis, 32(3): 775-780

Xu H, Zhang Y H, Hou W Z, Li L, Gu X F and Li Z Q. 2013. Monitoring haze in Beijing based on HJ-1 CCD. Journal of Remote Sensing, 2013, 17(2): 476-477

利用 HJ-1 CCD 高分辨率传感器反演灰霾气溶胶光学厚度

张玉环[1,2]，李正强[1]，侯伟真[1]，许华[1]

1.中国科学院遥感与数字地球研究所 国家环境保护卫星遥感重点实验室，北京 100101;
2.中国科学院大学，北京 100049

摘 要:霾已成为目前中国城市地区主要的空气污染现象,且近年来呈多发趋势。卫星遥感是获取大范围观测数据的必要手段,可对大气灰霾污染的分布区域及强度进行快速监测,弥补传统监测手段的不足。中国发射的环境小卫星(HJ-1)由于其高空间分辨率、较高的时间分辨率和宽覆盖等特点,在环境监测方面可发挥重要作用。本文在假设短时间内地表反射率稳定的基础上,用 HJ-1 CCD 影像蓝绿两个波段数据反演 2013 年 1 月北京市区灰霾天气的气溶胶光学厚度,对环境小卫星在灰霾天气的应用情况进行评价,并分析了高分辨率卫星遥感在灰霾监测中的可行性及优势。

关键词:高分辨率,气溶胶光学厚度,北京,霾,HJ-1 CCD

中图分类号:TP751 **文献标志码**:A

引用格式:张玉环,李正强,侯伟真,许华.2013.利用 HJ-1 CCD 高分辨率传感器反演灰霾气溶胶光学厚度.遥感学报,17(4):959-969

Zhang Y H, Li Z Q, Hou W Z and Xu H. 2013. Retrieval of haze aerosol optical depth based on high spatial resolution CCD of HJ-1. Journal of Remote Sensing, 17(4): 959-969 [DOI: 10.11834/jrs.20133062]

1 引 言

霾是由烟尘、粉尘等颗粒物在特定湿度、温度下与大气组成的气溶胶系统。颗粒物粒径主要在 0.1—10 μm 分布,其来源有风沙尘土、火山爆发、森林火灾等自然原因,也有工业排放、建筑工程、垃圾焚烧、生活废气以及汽车尾气等人为原因(马国欣等,2008)。国际气象组织 WMO 将空气相对湿度小于 80% 且水平能见度小于 10 km 的天气称为霾。霾根据能见度可分为 3 级:重霾(能见度≤2 km),中霾(2 km<能见度≤5 km),轻霾(5 km<能见度≤10 km)。

目前,中国灰霾形式相当严峻,许多城市都相继产生了灰霾现象。从大的区域范围来看,中国存在着 4 个灰霾情况严重的地区:珠江三角洲、长江三角洲、黄淮海地区和四川盆地。灰霾天气是一种严重的灾害性天气现象,对环境及人类健康的影响日益严重。它可以进入呼吸系统,引起人类呼吸和肺部疾病;可以降低大气能见度,影响城市空气质量,导致太阳辐射强度减弱与日照时数减少,造成农业减产等(李新妹和于兴娜,2011)。

目前环保部门主要从空气质量的角度关注霾天近地面的可吸入颗粒物浓度、污染气体 NO_2 和 SO_2 浓度。这些近地面“点”尺度的监测,虽然可以及时了解监测点附近的霾天污染状况,但缺乏对大尺度霾气溶胶光学厚度的监测能力(李莘莘,2010),因此很难获取大区域的灰霾分布范围及强度趋势等数据。卫星遥感具有覆盖面广,获取数据快速方便等特点,可以快速获取大区域的霾的气溶胶光学厚度等数据,可用于大气环境的监测。

目前比较成熟的卫星气溶胶光学厚度反演算法主要有以下几类:(1)基于中红外通道(2.12 μm)与

收稿日期:2013-03-21;**修订日期**:2013-05-10;**优先数字出版日期**:2013-05-17

基金项目:国家重大科学研究计划(编号:2010CB950800, 2010CB950801);中国科学院科技创新重点部署项目(编号:KGFZD-125-13-006)

第一作者简介:张玉环(1984—),女,博士研究生,现从事大气气溶胶的反演研究。E-mail: zhangyh@irsa.ac.cn

通信作者简介:李正强(1977—),男,研究员,主要从事大气遥感及大气环境研究。E-mail:lizq@irsa.ac.cn

红(0.66 μm)、蓝(0.47 μm)通道关系的暗目标法；此方法已成功应用于 MODIS 气溶胶反演(Levy 等，2007)；(2)基于多角度观测的多角度方法，MISR 气溶胶产品应用了此方法(Martonchik 和 Dine，1992)；(3)基于地表反射率的结构函数法(Tanre 等，1998)；(4)根据偏振信息的偏振气溶胶反演方法(POLDER)(Deuzé 等，2001)。

环境一号遥感卫星是中国发射的专门用于环境与灾害的监测预报卫星，此卫星上搭载的 CCD 传感器有 3 个可见光波段(430—520 nm，520—600 nm，630—690 nm)和一个近红外波段(760—900 nm)，分辨率为 30 m，幅宽为 360 km(双星联合可达 700 km)，重访周期为 4 天(双星联合为 2 天)。HJ 小卫星的高时间分辨率、高空间分辨率和宽覆盖的特点可使其在大气监测方面发挥重要作用。因此利用此卫星进行大气环境监测研究，发展基于此卫星的遥感监测方法具有重要意义(Wang 等，2010)。李莘莘(2010)分别用 MODIS 数据和环境小卫星 CCD 数据探讨了霾的识别及光学厚度反演方法；王中挺等人(2012)利用环境小卫星 CCD 影像对北京市 2009 年度的霾现象进行了研究；许华等人(2013)针对 2013 年 1 月 14 日(灰霾天气)和 17 日(晴朗天气)的气溶胶光学厚度做了简要介绍。本文针对整个灰霾过程的环境小卫星 CCD 影像，介绍气溶胶反演技术方法及多时相气溶胶光学厚度(AOD)结果，并和低分辨率 MODIS 的气溶胶产品进行对比分析。

2 原理与方法

2.1 基本原理

卫星遥感陆地上空气溶胶光学厚度发展于大气上界观测表观反射率，假设卫星观测的目标表面为均匀朗伯表面，不考虑气体吸收，那么卫星观测的表观反射率为：

$$\rho_{\mathrm{TOA}}(\mu_s,\mu_v,\phi)=\rho_o(\mu_s,\mu_v,\phi)+\frac{T(\mu_s)T(\mu_v)\rho_s(\mu_s,\mu_v,\phi)}{1-\rho_s(\mu_s,\mu_v,\phi)S} \quad (1)$$

式中，ρ_{TOA} 是大气顶部反射率；θ_v、θ_s 分别为观测天顶角与太阳天顶角；ρ_0 是大气的路径辐射项等效反射率；$T(\theta_s)$ 和 $T(\theta_v)$ 分别为向下和向上整层大气透过率；S 为大气的球面反照率；ρ 为地表反射率。

T 可以分为直射和散射两部分：$T(\mu)=\mathrm{e}^{-\tau/\mu}+t_d(\mu)$，$\tau$ 是总体光学厚度，t_d 是散射透射率。其中，卫星接收到的总辐射包括来自地表和大气的两部分，程辐射项主要是来自大气贡献的部分。

气溶胶反演的核心是进行地气分离，即下垫面反射率贡献的去除。根据不同的地气分离方法，发展了不同的气溶胶反演方法。本研究进行气溶胶光学厚度反演时，选取 6S(Second Simulation of Satellite Signal in the Solar Spectrum)辐射传输模式(Vermote 等，1997)对大气和地表对卫星接收信号的影响进行模拟，根据地表反射率的假设进行地气分离，达到获取气溶胶信息的目的。

2.2 HJ-1 AOD 反演方法

本研究的 AOD 反演建立在以下两个假设的基础上：(1)大气气溶胶随时间变化迅速，随地点变化缓慢，可假定在一个较小的区域内，气溶胶光学厚度是不变的；(2)地表反射率随地点变化迅速随时间变化缓慢，即在一个较短的时间段内，地表反射率变化微小。基于以上两个假设，相邻时相的遥感影像表观辐亮度的变化来自于不同时间的大气对太阳辐射不同程度的影响。在地表反射率稳定的基础上根据表观辐亮度的变化来进行地气分离，获取气溶胶光学厚度和地表反射率数据。具体步骤如下：

(1)根据所选研究区域和卫星数据参数建立查找表。应用已有的 6S 辐射传输模型，查找表中考虑了太阳天顶角、太阳方位角、观测天顶角、观测方位角、气溶胶光学厚度和地表反射率等参数，并且应用了 6S 自带的大气模式(中纬度夏季、中纬度冬季)和气溶胶模型参数(大陆型气溶胶、城市型气溶胶等)。

灰霾天和晴朗天 AOD 反演的差异主要在气溶胶模型参数的选择上，有研究表明(Li 等，2013)灰霾天气气溶胶模型参数与大陆型气溶胶模型参数最为接近，只是灰霾天气气溶胶浓度比一般天气要大，因此，本研究反演灰霾天气气溶胶光学厚度时采用的气溶胶模型为大陆型气溶胶。

(2)根据卫星影像的表观辐亮度数据及观测-太阳几何查找出在不同气溶胶情况下对应的地表反射率数据。此处的 AOD 为假设值。

(3)根据地表反射率稳定的假设，对地表反射率进行判断，取相邻两时相图像地表反射率最接近的情况对应的 AOD 分别作为此两时相图像的真实 AOD。

式(2)用于判断地表反射率，该公式取最小值

时判定为地表反射率最接近情况(Hagolle 等,2008)。

$$Cost = K\sum_{i,j,\lambda}(atm_{cor}(L_{TOA}(i,j,\lambda,D1),\mathrm{AOD}(D1)) - atm_{cor}(L_{TOA}(i,j,\lambda,D2),\mathrm{AOD}(D2)))^2 + \sum_{i,j,\lambda}(atm_{cor}(L_{TOA}(i,j,\lambda,D1),\mathrm{AOD}(D1)) - \rho_{surf}(i,j,\lambda,D1))^2 + \sum_{i,j,\lambda}(atm_{cor}(L_{TOA}(i,j,\lambda,D2),\mathrm{AOD}(D2)) - \rho_{surf}(i,j,\lambda,D1))^2 \quad (2)$$

式中,λ 为波长;(i,j)是图像中选定的子区域的像元坐标,在此子区域内,认为 AOD 没有发生变化;L_{TOA} 是表观辐亮度;atm_{cor} 是基于查找表在表观辐亮度为 L_{TOA} 对应气溶胶光学厚度为 AOD($D2$)时的地表反射率数据;ρ_{surf} 为初始地表反射率;$D1$、$D2$,表示时间序列图像的第 $D1$ 天和第 $D2$ 天。假设所选取的时间序列图像 $D1$、$D2$ 在所选区域内是无云的(如果 $D2$ 天有云的,也可以去 $D3$、$D4$ 等),在一个短的时间间隔内,地表反射率基本不变,通过求取上述价值函数(式(2))的最小值即可获取第 $D1$ 和第 $D2$ 天的 AOD 以及对应的地表反射率数据。

HJ-1 CCD 传感器设置有 4 个波段,相对于其他几个波段来说,蓝光(中心波长为 0.48 μm)、绿光(中心波长为 0.56 μm)波段对气溶胶的效应比较敏感,并且在大多数情况下,此波段的地表反射率变化缓慢。因此,本研究中仅用到了 HJ-1 CCD 的蓝光波段和绿光波段进行 AOD 反演。4 个传感器的波段响应函数如图 1 所示。

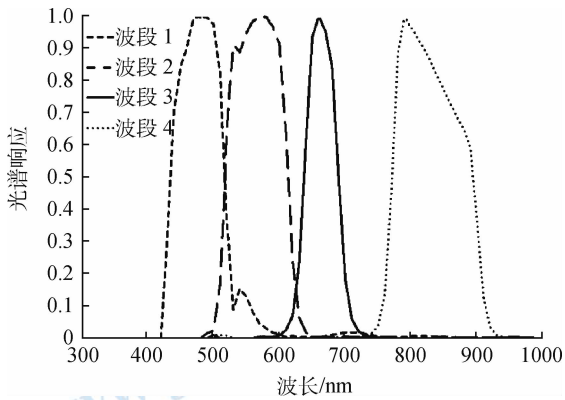

图 1 环境小卫星 CCD 传感器各波段的光谱响应函数
(以 HJ-1 A 星 CCD1 为例)

2.3 云判定及去除

霾光学厚度反演前首先要进行霾像元识别,霾、云、地表像元的检测精度将直接影响到反演结果。目前许多卫星都已经有了比较成熟的云检测算法,但由于 HJ-1 CCD 传感器只有 3 个可见光波段和一个近红外波段,在云检测时,参考已有研究成果,将 HJ-1 CCD 蓝光波段的反射率阈值设定为[0.07,0.25],红光波段的反射率阈值设定为[0.1,0.28],这一阈值范围在保证大部分厚云被排除的同时,防止了将较重的霾及较亮的地物误判为云(Ackerman,2010; 李莘莘,2010),用此简单的阈值方法对选定研究区域的数据进行云的判定,判定为云的情况将云区域进行掩膜处理,不进行 AOD 反演。

3 霾天 AOD 反演结果及分析

3.1 数据选取及处理

选取 2013 年 1 月 8 日至 17 日第 2 次灰霾天气过程中的无云的 HJ-1 CCD 数据,共有 6 景图像(表 1),其中 2013 年 1 月 8 日图像为灰霾开始时的图像,当天北京市东三环北路全国农业展览馆站点空气质量指数 AQI 为 158,2013 年 1 月 12 日和 14 日为灰霾严重时的图像,AQI 分别为 500 和 293,2013 年 1 月 17 日为灰霾消散后的卫星遥感影像,AQI 为 106。此系列图像正好表示了北京市区一个灰霾天气的产生、发展、积聚和消散的过程。

表 1 数据选取

日期	传感器	过境时间
2013-01-08	HJ-1A CCD1	02:37
2013-01-10	HJ-1B CCD1	02:36
2013-01-12	HJ-1A CCD1	02:42
2013-01-14	HJ-1B CCD1	02:41
2013-01-16	HJ-1A CCD1	02:46
2013-01-17	HJ-1B CCD2	02:20

将所选研究区域的图像进行几何配准,裁剪出北京市区作为研究区域,面积为 20×20 km^2,在 HJ-1 CCD 影像上为 666×666 像元。图 2 为所选研究区域的标准假彩色合成图像。图中红框处为 CE318(太阳光度计)所在站点位置(中国科学院遥感与数字地球研究所站)。

为了提高信噪比和减少几何校正误差,将 HJ-1 CCD 30 m 分辨率图像重采样成 100 m 分辨率(200×200 像元),然后将研究区的数据进行辐射定标处理,获取表观辐亮度图像。在 100 m 分辨率影像中,认为 5×5 个像元(0.5 km×0.5 km)区域内气溶胶特性是稳定的。如式(2)中,i、j 的最大值设为 5,即选择

500 m 作为反演的 AOD 结果的空间分辨率。

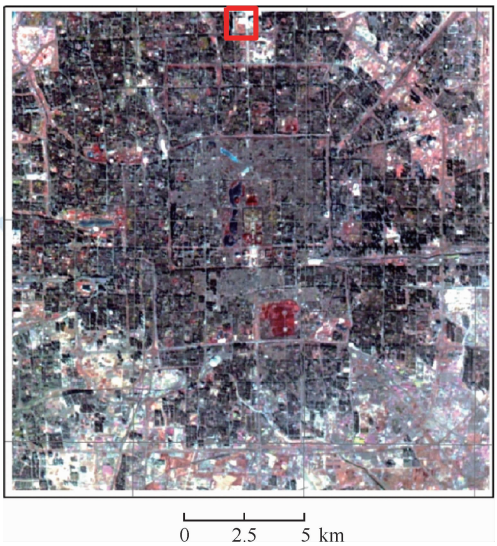

图 2 HJ-1 CCD 影像研究区域
(北京市区,20×20 km^2)

3.2 反演结果

图 3 是 2013 年 1 月 8 日至 17 日第 2 次灰霾期间,HJ-1 CCD 传感器反演 AOD 结果图。其中初始地表反射图像选取时间序列图像中的第 1 景晴朗无云图像(2013 年 1 月 8 日图像),对前两个波段进行辐射定标和大气校正后得到的地表反射率图像。结果图中 2013 年 1 月 12 日图像和 2013 年 1 月 10 日图像中的 0 值区域为无效值,是判定为云后掩膜掉的区域。

HJ-1 A 星和 B 星联合,达到了 2 天一次的观测频率,此反演结果清晰呈现了整个灰霾过程的发生、发展、积聚和逐步消散过程。

由以上结果可以看出,北京市区 2013 年 1 月份第 2 次灰霾期间(2013 年 1 月 8 日至 17 日),8 日为灰霾开始时间,当天所取研究区域北京市区卫星过

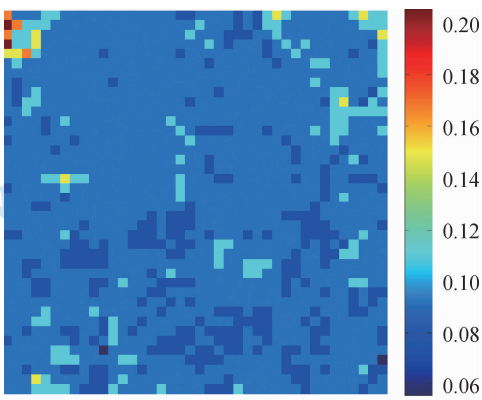

(a) 2013-01-08

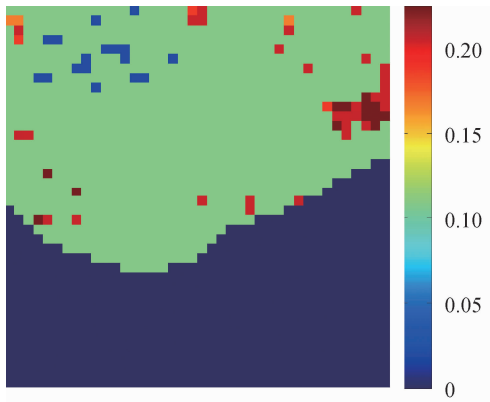

(b) 2013-01-10

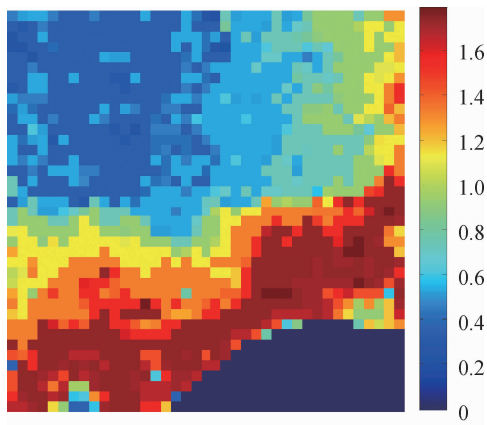

(c) 2013-01-12

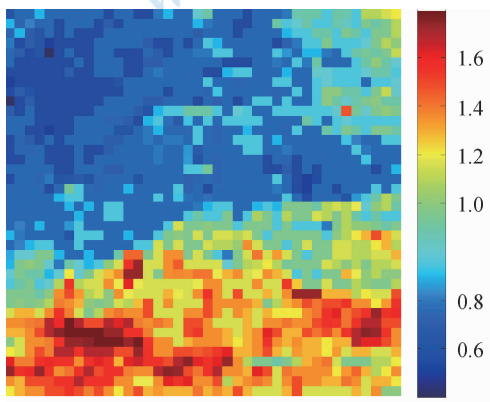

(d) 2013-01-14

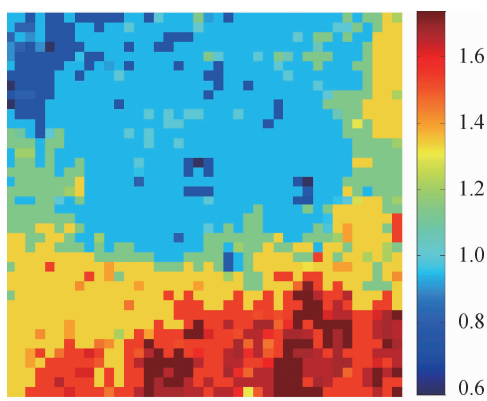

(e) 2013-01-16

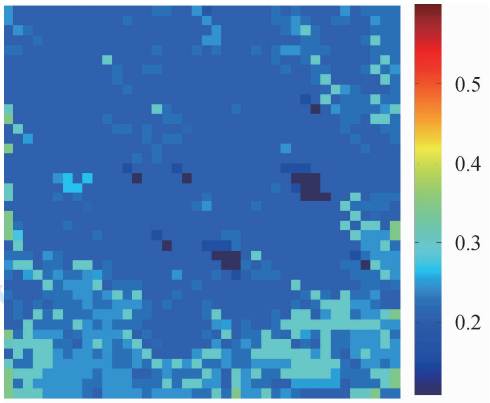

(f) 2013-01-17

图 3 2013 年 1 月 8 日—17 日 AOD 反演结果

境时刻的平均 AOD 反演结果约为 0.1,且整体区域变化较小,AOD 最大差异小于 0.15;10 日为灰霾的发展阶段,10 日图像虽南半部分有云的干扰,但是北部无云区域的 AOD 已经明显高于 8 日反演结果,反映了一个灰霾的积聚过程,12 日反演结果 AOD 继续增大,整体高于 10 日结果,并且南部区域反演结果明显高于北部反演结果,南北部 AOD 差异高达 1.4 左右,此时灰霾积聚明显,是一个严重的灰霾天气;14 日也是严重灰霾天气,南部一些地区灰霾向北部扩散,北部地区 AOD 反演结果明显高于 12 日结果,南部地区 AOD 最大值在 1.6 左右,与 12 日结果类似。16 日为灰霾消散的阶段,从反演结果图上可以看出,16 日 AOD 结果整体明显低于 14 日反演结果,东北部地区 AOD 由 14 日的 1.7 左右下降到 1.4 左右,南部区域由 14 日的 0.9 左右下降到 0.6 左右;17 日此灰霾过程结束,研究区域内 AOD 反演结果整体小于 0.35。

3.3 AOD 反演结果对比验证

(1)AOD 反演结果与 CE318 实测结果验证

根据中国科学院遥感与数字地球研究所 CE318 站点实测 AOD 结果和 Ångström 参数公式(式(3)),利用 CE318 实测的 440 nm 和 870 nm 处的 AOD,计算出 550 nm 处的 AOD,并与 HJ-1 CCD 反演的 AOD 结果进行对比(Dubovik 等,2000; Ångström,1929)。其中,CE318 实测值选取卫星过境时刻的测量值。

$$\tau_\alpha(\lambda)=\beta\lambda^{-\alpha} \tag{3}$$

式中,$\tau_\alpha(\lambda)$是 550 nm 处的气溶胶光学厚度,β 是气溶胶浊度系数;α 是 Angstrom 指数,反映粒子大小,值越大气溶胶粒子越小。

表 2 为实测结果和反演结果对比。通过表 2 可以看出,HJ-1 CCD 反演结果与 CE318 实测站点观测结果相比,6 天的平均 AOD 差异为 0.002,各天 AOD 反演结果与实测结果的平均误差为 0.095。反演结果中误差最大的为 2013 年 1 月 10 日的图像,误差为 0.252,误差最小的为 2013 年 1 月 14 日的图像,误差为 0.007。实测结果与 HJ-1 CCD 反演结果的相关性公式为:$\tau_{HJ}=1.083\times\tau_{CE318}-0.030$,$R^2$ 为 0.84。

表 2 HJ-1 CCD 反演结果验证

日期	CE318-AOD	HJ-1 AOD	误差
2013-01-08	0.102	0.074	0.026
2013-01-10	0.412	0.160	0.252
2013-01-12	0.365	0.420	0.055
2013-01-14	0.858	0.940	0.082
2013-01-16	0.467	0.560	0.093
2013-01-17	0.138	0.200	0.062
平均值	0.390	0.392	0.095

(2)反演结果与 MODIS 气溶胶产品对比分析

由于霾天发生时,MODIS 云掩码产品和气溶胶产品通常将霾作为薄云、雾或者亮目标处理(King,2003 等; Liang 等,2006),导致反演结果缺失或不准确。在 2013 年 1 月北京地区灰霾期间,尤其是第二次重灰霾(2013 年 1 月 8 日至 2013 年 1 月 17 日)期间,MODIS 气溶胶产品缺失。MOD08(MOD08:大气 3 级标准数据产品,内容为栅格大气产品,空间分辨率为 1 km。每日、每旬、每月合成数据)产品存在大量的缺失。极大的限制了该卫星气溶胶遥感在监测区域霾天气中的应用。另外,低空间分辨率的气溶胶在小区域灰霾监测上也不占有优势,在本文所选的研究区域北京市区,相对于 MODIS 1 km 空间分辨率来说,20×20 个像元的结果对详细描述霾的空间分布趋势来说也是不够的。

4 结 论

由 HJ-1 CCD 反演的 AOD 结果可以明显看出,2013 年 1 月 8 日—17 日期间灰霾在北京市区的整个发展、聚集和消散过程,以及成像时霾的强度及分布范围。因此,HJ-1 CCD 影像的高空间分辨率、高时间分辨率等特性使其具有监测霾天气 AOD 的优势。由以上分析我们可以得出:

(1)在北京市区 2013 年 1 月 8 日—17 日严重灰霾污染过程中,霾的趋势大体上是由南向北推进,8

日、10 日开始发展，12 日、14 日达到最高值，16 日开始消散，17 日接近清洁。

(2)由 12 日和 14 日的 AOD 区域分布图可以看出，灰霾污染从北京城南地区逐渐向北部侵袭发展，灰霾期间南部灰霾持续比北部严重，并呈从南部向两侧外扩，逐渐包围北部的趋势。南部 AOD 反演结果明显高于北部地区，并且 AOD 的值由南至北，逐渐减小。

卫星遥感监测结果表明，卫星遥感技术作为一种新型的监测手段，可有力补充地面监测的不足，实时、快速地实现大范围的灰霾立体监测，提供灰霾影响范围、严重程度及分布等技术指标。

志　谢　本文中的 AQI 数据为北京市环境保护局网站提供，在此表示感谢。

参考文献(References)

Ackerman S, Frey R, Strabala K, Liu Y, Gumley L, and Baum B. 1998. Discriminating clear sky from clouds with MODIS. Journal of Geophysical Research: Atmospheres (1984—2012), 103(D24): 32141-32157

Ångström A. 1929. On the atmospheric transmission of sun radiation and on dust in the air. Geografiska Annaler, 11: 156-165

Deuzé J L, Bréon F M, Devaux C, Goloub P, Herman M, Lafrance B, Maignan F, Marchand A, Nadal F, Perry G and Tanré D. 2001. Remote sensing of aerosols over land surfaces from POLDER-ADEOS-1 polarized measurements. Journal of Geophysical Research, 106(1996): 4913-4926 [DOI: 10.1029/2000JD900364]

Dubovik O and King M D. 2000. A flexible inversion algorithm for retrieval of aerosol optical properties from sun and sky radiance measurements. Journal of Geophysical Research, 105(D16): 20673-20696 [DOI: 10.1029/2000JD900282]

Hagolle O, Dedieu G, Mougenot B Debaecker V, Duchemin B and Meygret A. 2008. Correction of aerosol effects on multi-temporal images acquired with constant viewing angles: Application to Formosat-2 images. Remote Sensing of Environment, 112(4): 1689 - 1071 [DOI: 10.1016%2fj.rse.2007.08.016]

King M D, Menzel W P, Kaufman Y J, Tanre D, Platnick S, Ackerman S A, Remer L A, Pincus R and Hubanks P. 2003. Cloud and aerosol properties, precipitable water, and profiles of temperature and water vapor from MODIS. IEEE Transactions on Geoscience and Remote Sensing, 41(2): 442-458 [DOI: 10.1109/TGRS.2002.808226]

Levy R C, Remer L A, Mattoo S, Vermote E F and Kaufman Y J. 2007. Second-generation operational algorithm: retrieval of aerosol properties over land from inversion of Moderate Resolution Imaging Spectroradiometer spectral reflectance. Journal of Geophysical Research, 112(D13): 1-21 [DOI: 10.1029/2006JD007811]

Liang S L, Zhong B and Fang H L. 2006. Improved estimation of aerosol optical depth from MODIS imagery over land surfaces. Remote Sensing of Environment, 104(4): 416-425

李莘莘. 2010. 霾气溶胶光学厚度卫星遥感反演算法研究. 中国科学院研究生院博士学位论文

李新妹, 于兴娜. 2011. 灰霾期间气溶胶化学特性研究进展. 中国科技论文在线, 6(9): 661-664

Li Z Q, Gu X, Wang L, Li D, Li K, Dubovik O, Schuster G, Goloub P, Zhang Y, Li L, Xie Y, Ma Y and Xu H. 2013. Aerosol physical and chemical properties retrieved from ground-based remote sensing measurements during heavy haze days in Beijing winter. Atmospheric Chemistry and Physics Discussions, 13(2): 5091-5122 [DOI: 10.5194/acpd-13-5091-2013]

马国欣, 薛永祺, 李高丰. 2008. 珠江三角洲地区的灰霾监控与卫星遥感. 科技导报, 26(16): 72-76

Martonchik J V and Dine D J. 1992. Retrieval of aerosol optical properties from multi-angle satellite imagery. IEEE Transactions on Geoscience and Remote Sensing, 30(2): 223-230 [DOI:10.1109/36.134073]

Tanre D, Deschamps P Y, Devaux C and Herman M. 1988. Estimation of Saharan aerosol optical thickness from blurring effects in Thematic Mapper data. Journal of Geophysical Research, 93(D12): 15955-15964 [DOI: 10.1029/JD093iD12p15955]

Vermote E F, Tanre D, Deuze J L, Herman M and Morcette J J. 1997. Second simulation of the satellite signal in the solar spectrum, 6S: an overview. IEEE Transactions on Geoscience and Remote Sensing, 35(3): 675-686 [DOI: 10.1109/36.581987]

Wang Q, Wu C Q and Li Q. 2010. Environment Satellite 1 and its application in environmental monitoring. Journal of Remote Sensing, 14(1): 104-121

王中挺, 厉青, 李莘莘, 陈良富, 周春艳, 王子峰, 张丽娟. 2012. 基于环境一号卫星的霾监测应用. 光谱学与光谱分析, 32(3): 775-780

许华, 张玉环, 侯伟真, 吕阳, 李莉, 顾行发, 李正强. 2013. 利用环境一号卫星监测北京地区雾霾. 遥感学报, 17(2): 476-477

遥感学报

启功先生创刊题名

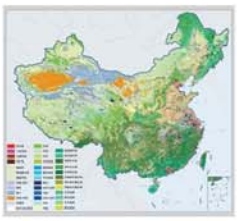

封面说明

About the Cover

2010年中国土地覆被遥感监测数据集（ChinaCover2010）

The China National Land Cover Data for 2010 (ChinaCover2010)

2010年中国土地覆被遥感监测数据集（ChinaCover2010）由中国科学院遥感与数字地球研究所联合其他9个单位历时两年完成，应用30 m空间分辨率的环境星（HJ-1A/1B）数据，利用联合国粮农组织（FAO）的LCCS分类工具，构建了适用于中国生态特征的38类土地覆被分类系统，采用基于超算平台的数据预处理、面向对象的自动分类、地面调查获得的10万个野外样本以及雷达数据辅助分类相结合的方法，数据精度达到85%。ChinaCover2010主要基于国产卫星影像，将遥感与生态紧密结合，充足的野外样点以及严格的产品质量控制在最大程度上保证了数据的精度，可为中国生态环境变化评估以及生态系统碳估算提供基础数据支撑。（网址：http://www.chinacover.org.cn）

The China National Land Cover Data for 2010 (ChinaCover2010) has been completed after two years of team effort by the Institute of Remote Sensing and Digital Earth (RADI), Chinese Academy of Sciences (CAS), together with nine other institutions' participation. The HJ-1A/1B satellite at 30 m resolution is main data source. Based on the landscape features in China, 38 land cover classes have been defined using UN FAO Land Cover Classification System (LCCS). Super computers were used in the data preprocessing. An object-oriented method and a thorough field survey (about 100000 field samples) were used in the land cover classification, with radar imagery as auxiliary data. The overall accuracy of ChinaCover2010 is around 85%. Mainly based on domestic imagery, the products take advantage of various in situ data and strict quality control. ChinaCover2010 is a good dataset for ecological environment change assessment and terrestrial carbon budget studies. (Website: http://www.chinacover.org.cn)

遥感学报

JOURNAL OF REMOTE SENSING

YAOGAN XUEBAO（双月刊　1997年创刊）

第17卷　第4期　2013年7月25日

(Bimonthly, Started in 1997)

Vol.17 No.4 July 25, 2013

主　管	中国科学院	Superintended by	Chinese Academy of Sciences
主　办	中国科学院遥感与数字地球研究所 中国地理学会环境遥感分会	Sponsored by	Institute of Remote Sensing and Digital Earth,CAS The Associate on Environment Remote Sensing of China
主　编	顾行发	Editor-in-Chief	GU Xing-fa
编　辑	《遥感学报》编委会 北京市安外大屯路中国科学院遥感与数字地球研究所 邮编：100101　电话：86-10-64806643 http://www.jors.cn E-mail:jrs@irsa.ac.cn	Edited by	Editorial Board of Journal of Remote Sensing Add: P.O.Box 9718, Beijing 100101, China Tel: 86-10-64806643 http://www.jors.cn E-mail: jrs@irsa.ac.cn
出　版	科学出版社	Published by	Science Press
印刷装订	北京科信印刷有限公司	Printed by	Beijing Kexin Printing Co. Ltd.
总 发 行	科学出版社 北京东黄城根北街16号 邮政编码：100717 电话：86-10-64017032 E-mail:sales_journal@mail.sciencep.com	Distributed by	Science Press Add: 16 Donghuangchenggen North Street, Beijing 100717, China Tel: 86-10-64017032 E-mail: sales_journal@mail.sciencep.com
国外发行	中国国际图书贸易总公司 北京399信箱　邮政编码：100044	Overseas distributed by	China International Book Trading Corporation Add: P.O.Box 399, Beijing 100044, China

中国标准连续出版物号：ISSN 1007-4619 / CN 11-3841/TP

CODEN YXAUAB

国内邮发代号：82-324

国外发行代号：BM 1002

定价：70.00元

ISSN 1007-4619

国内外公开发行